This is the author's version of an article that has been published in this journal. Changes were made to this version by the publisher prior to publication.
The final version of record is available at http://dx.doi.org/10.1109/TSG.2016.2631448

Wide-Area Damping Control using Multiple DFIG-based Wind Farms Under Stochastic Data Packet Dropouts

Amirthagunaraj Yogarathinam, *Student Member, IEEE*, and Nilanjan Ray Chaudhuri, *Senior Member, IEEE*

***Abstract*—Data dropouts in communication network can have a significant impact on wide-area oscillation damping control of a smart power grid with large-scale deployment of distributed and networked Phasor Measurement Units (PMUs) and wind energy resources. Remote feedback signals sent through communication channels encounter data dropout, which is represented by the Gilbert-Elliott model. An Observer-driven Reduced Copy (ORC) approach is presented, which uses the knowledge of the nominal system dynamics during data dropouts to improve the damping performance where conventional feedback would suffer. An expression for the expectation of the bound on the error norm between the actual and the estimated states relating uncertainties in the cyber system due to data dropout and physical system due to change in operating conditions is also derived. The key contribution comes from the analytical derivation of the impact of coupling between the cyber and the physical layer on ORC performance. Monte Carlo simulation is performed to calculate the dispersion of the error bound. Nonlinear time-domain simulations demonstrate that the ORC produces significantly better performance compared to conventional feedback under higher data drop situations.**

***Index Terms*—Networked Control Systems (NCS), Cyber-Physical System (CPS), Smart Grid, Phasor Measurement Unit (PMU), Wide-area Measurement, Electromechanical Oscillations, Observer-driven Reduced Copy (ORC), Wind Farm, Data-dropouts, Gilbert-Elliott Model.**

List of Symbols

R_r/R_s	Rotor/Stator resistance of DFIG.
L_r/L_s	Rotor/Stator leakage inductance of DFIG.
L_m	Mutual inductance of DFIG.
R_{fr}/R_{fg}	RSC/GSC filter resistance of DFIG.
L_{fr}/L_{fg}	RSC/GSC filter inductance of DFIG.
i_{qr}, i_{dr}	q/d-axis RSC current of DFIG.
i_{qg}, i_{dg}	q/d-axis GSC current of DFIG.
i_{qr}/i_{dr}	q/d-axis RSC current of DFIG.
v_{qs}/v_{ds}	q/d-axis DFIG bus voltage of DFIG.
v_{qt}/v_{dt}	q/d-axis RSC voltage of DFIG.
v_{qg}/v_{dg}	q/d-axis GSC voltage of DFIG.
s_{r1}, s_{r2}	RSC current controller states.
s_{g1}, s_{g2}	GSC current controller states.
K_{ir}, K_{pr}	RSC controller parameters.
K_{ig}, K_{pg}	GSC controller parameters.
$K_v(s)$	DC voltage controller.
K/L	State feedback/observer gain vector.
$\bar{x}$	State vector estimated by the observer at the sensor location for the case of ORC.
x_n	State vector estimated by reduced copy.
$\bar{\bar{x}}$	State vector received by the receiver.
x_i	State vector of the reduced power system under off-nominal condition.
t_k	Instant of the state resetting of reduced copies
x^0_{nk}	Reduced copy estimated state at time t_k.
x^0_{ik}	Actual state of reduced power system model at time t_k.
$\bar{x}_k$	Observer estimated state at time t_k for ORC.
$u(t)$	Control input to the actuator for ORC.
y_m	Feedback signal from the PMU location.
$\bar{y}_m$	Feedback signal received by the receiver
$\bar{x}_{ob}$	State vector estimated by the observer at the actuator location for the case of CFC.
$\bar{u}(t)$	Control input calculated at the actuator location for the case of CFC.
$\mathbf{\Psi_k}$	Binary diagonal random matrix.
R/ρ	Data receiving rate as % / fraction.
$\tilde{A}, \tilde{B}, \tilde{C}$	Deviation in actual operating condition from nominal.
$\xi(t)$	Error between the reduced order power system state trajectory and that of reduced copy.
$\|\cdot\|$	Euclidian norm of a vector or a matrix.
$\mathbf{E}[\|\xi(t)\|]$	Expected value of $\|\xi(t)\|$.
K_1, K_2, K_3	Proportionality constants.
$\times$	Matrix multiplication sign.

The authors are with Department of Electrical Engineering, The Pennsylvania State University, State College, PA, USA (e-mail: *axy43@psu.edu, nuc88@engr.psu.edu*).

Financial support from NSF under grant award # 1657024 is gratefully acknowledged.

I. Introduction

THE 2010 American Physical Society's Panel on Public Affairs (POPA) reported [1] that land-based wind energy totals more than 8000 GWs of potential capacity. Although small amount of renewable generation can be easily integrated into the grid, accommodating large penetration from these renewable sources will require new approaches to enable reliable operation of the grid. The Networked Control System (NCS) with distributed networked sensors (i.e. Phasor Measurement Units (PMUs)) has the potential to be a key enabler towards achieving this objective. In a NCS the control and the feedback signals are exchanged amongst a multitude of sensors and actuators through a communication network in the form of data packets. However in a power system with large geographical span leading to huge separation of the sensors and the actuators, the challenges of maintaining

Copyright (c) 2017 IEEE. Personal use is permitted. For any other purposes, permission must be obtained from the IEEE by emailing pubs-permissions@ieee.org.

This is the author's version of an article that has been published in this journal. Changes were made to this version by the publisher prior to publication.
The final version of record is available at http://dx.doi.org/10.1109/TSG.2016.2631448

TABLE I
SUMMARY OF EXISTING POWER SYSTEMS LITERATURE AND GAPS

References	*Data drop*	*Communication model*	*Comments*
[8] – [10]	*not considered*	*latency considered*	*unmodeled stochastic data drop in cyber layer*
[11]	*–do–*	*deterministic : low data rate*	*–do–*
[12]	*considerd*	*Bernoulli*	*accuracy issues with congestion*

reliability within the NCS in the face of uncertainties such as network congestion, bandwidth limitations, data drop, packet corruption, latency and signal loss increases significantly.

Packet dropouts is a significant challenge for the NCSs which occurs from transmission errors in the physical layer (which is far more common in wireless than the wired networks) or from buffer overflows due to congestion. Dropout during the data transmission is unpredictable. Reliable transmission protocols, such as Transmission Control Protocol (TCP) which provides mechanisms for re-transmission (full-duplex) of lost data, guarantees the eventual delivery of packets whereas User Datagram Protocol (UDP) does not provide error recovery and flow control mechanisms, but in a NCS the re-transmission of old data is generally not very useful [2].

With NCS likely to be more common, the impact of data dropout on power oscillation damping controllers is a matter of concern. In the recent past many research papers [3]–[7] have been published in the area of NCS to model the impact of data dropouts, bandwidth (BW) restriction and delays in it, but the significance of combining communication constraints and control specification has not been addressed adequately in the power systems literature. In [8]–[10], doubly-fed induction generator (DFIG)-based wind farms (WFs) for wide-area power oscillation damping were proposed where latency in the communication layer was considered. In [11] the BW restriction in the communication network was dealt with in a deterministic framework. However, packet dropout was not considered in any of [8]–[11]. Singh *et-al* [12] represented packet data transmission process and the probability of packet loss using an independent Bernoulli model in NCS for power system control. However, as mentioned in [12], the validity of Bernoulli model is questionable when the communication channel is congested. Table I summarizes the gap in the existing power systems literature mentioned above.

In this paper, a Gilbert-Elliot model with detailed characterization of the communication process with packet loss probability has been considered in NCS framework for power system control. An observer-driven reduced copy (ORC) with linear quadratic regulator (LQR) based optimal control scheme is used to damp inter-area oscillations in the reduced equivalent model of the New England-New York power system using two DFIG-based WFs. The key contribution of this paper comes from the consideration of Gilbert-Elliot model of stochastic packet drop and the analytical derivation of the impact of interaction between the cyber and the physical layer on ORC performance in equation (36). Our work reveals that the uncertainty in the cyber layer due to data packet drop and the off-nominal operation of the physical layer due to outages etc. affect the performance in a coupled manner, where the coupling mechanism is non-trivial. The analytical results are verified through time-domain simulations.

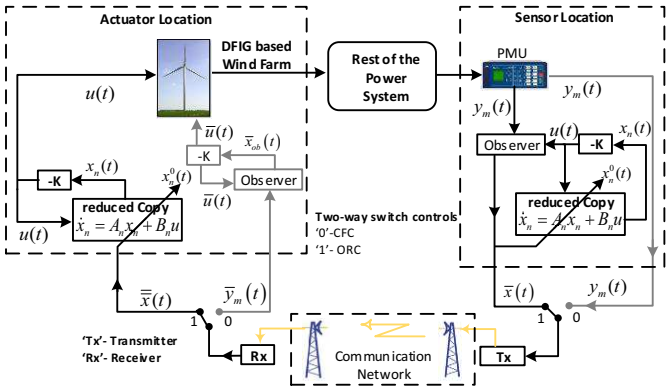

Fig. 1. Overall architecture of the NCPS including conventional feedback control (CFC) in gray and the proposed Observer-driven Reduced Copy (ORC).

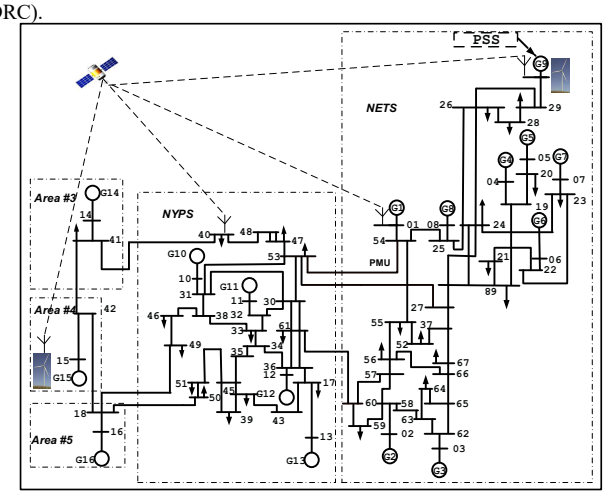

Fig. 2. 16-machine, 5-area equivalent representing New England - New York power system. Wind farms are connected to bus-9 and bus-15.

II. MODELING OF NETWORKED CONTROLLED POWER SYSTEM (NCPS)

Three main components of the Networked Controlled Power System (NCPS), Fig. 1, are the physical layer (i.e. power system), the cyber layer (i.e. communication network) and the controller, respectively. The following subsection discusses the modeling of the power system.

A. Power System Modeling

The nonlinear positive sequence fundamental frequency phasor model of a 16-machine 5-area dynamic equivalent of the New England-New York system is considered for the case study, see Fig. 2. All the Synchronous Generators (SGs) are represented by sixth-order subtransient models and eight of them (G1-G8) are equipped with the IEEE DC1A excitation system. The rest of the SGs are under manual excitation control, G9 is equipped with a static exciter and a power

Copyright (c) 2017 IEEE. Personal use is permitted. For any other purposes, permission must be obtained from the IEEE by emailing pubs-permissions@ieee.org.

This is the author's version of an article that has been published in this journal. Changes were made to this version by the publisher prior to publication.
The final version of record is available at http://dx.doi.org/10.1109/TSG.2016.2631448

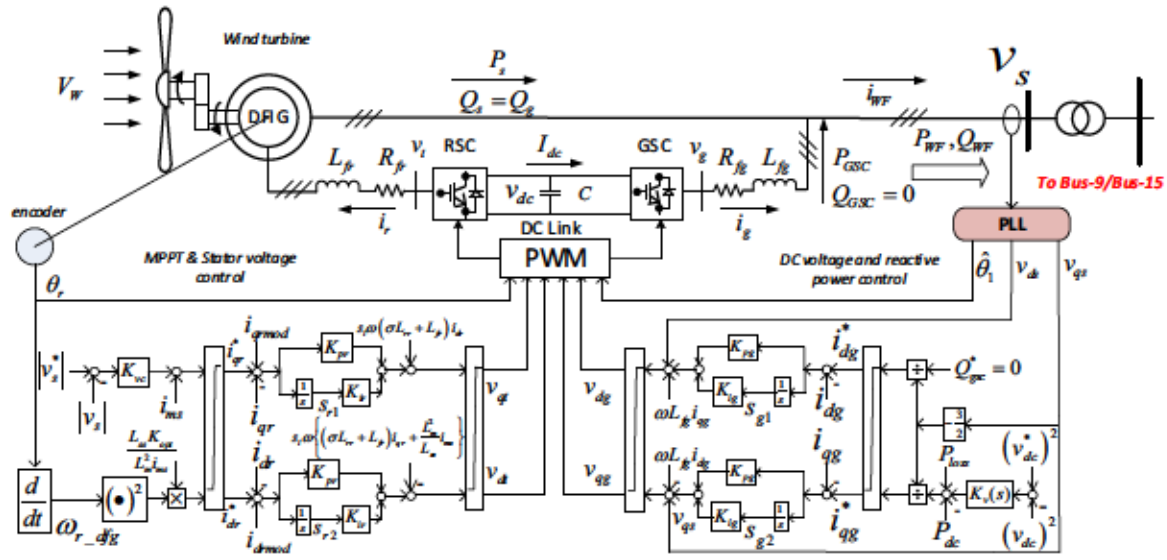

Fig. 3. Schematic of the DFIG-based WF with its controller. The WFs are connected to the power system as shown in Fig.2.

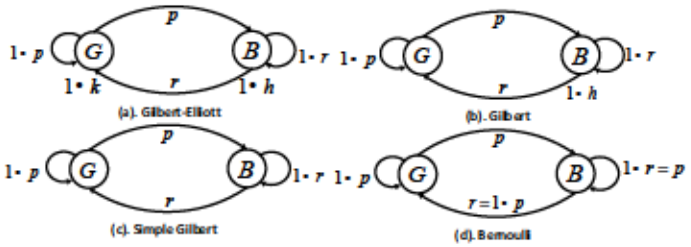

Fig. 4. Different data dropout models in the communication link.

system stabilizer (PSS). The active and reactive components of loads have constant impedance characteristics. The dynamic data of the power system and the nominal power transfer through tie lines can be found in [13]. In this paper, we will consider the impact of shutting down two conventional plants (G9 and G15) and replacing them with two equivalent DFIG-based WFs. Modeling of the WF is described next.

B. Wind Farm Modeling and Controls

The overal structure of a DFIG-based WF with its controls is shown in Fig. 3, which is represented by an aggregated model whose turbine-generator rotational dynamics is represented by a two-mass model to include the torsional mode. The generator is modeled using standard differential and algebraic equations as given in [14]. The turbine is assumed to operate in the zone of maximum power point extraction. Also, the blade pitch angle and the wind speed is assumed to be constant. The tie-reactors of the VSCs, DC-link dynamics and the PLL dynamics are included in the model (Fig. 3).

Standard vector control approach was considered for both rotor-side converter (RSC) and the grid-side converter (GSC) controls, as mentioned in [15]. For Maximum Power Point Tracking (MPPT) and stator terminal voltage control for the RSC (see Fig. 3), the stator flux is aligned with the q-axis. With the modified reference frame, simplified expressions for v_{dt} and v_{qt} are as follows:

$$\begin{aligned} v_{dt} &= -R_r i_{dr} - (\sigma L_{rr} + L_{fr})\tfrac{d(i_{dr})}{dt} - s_l\omega(\sigma L_{rr} + L_{fr})i_{qr} \\ &\quad -s_l\omega\tfrac{L_m^2}{L_{ss}} i_{ms} \\ v_{qt} &= -R_r i_{qr} - (\sigma L_{rr} + L_{fr})\tfrac{d(i_{qr})}{dt} + s_l\omega(\sigma L_{rr} + L_{fr})i_{dr} \end{aligned} \quad (1)$$

where, $\sigma = 1 - L_m^2/(L_{ss}L_{rr})$. The $d-$axis reference current i_{dr}^* for RSC is determined from the torque reference through the MPPT algorithm as follows:

$$T_m^* = \tfrac{L_m^2}{L_{ss}} i_{ms} i_{dr}^* = 0.5\rho\pi R_{tur}^5 \tfrac{C_{pot}}{\lambda_{opt}^3}\omega_{r\_dfg}^2 = K_{opt}\omega_{r\_dfg}^2 \quad (2)$$

where, C_{Popt} and λ_{opt} are the optimum power coefficient and optimum tip-speed-ratio of the turbine, respectively. The $q-$axis current reference i_{qr}^* ensures that the magnetizing current i_{ms} drawn by the induction machine is supplied through the RSC while injecting/absorbing appropriate reactive power depending on the difference between actual $|V_s|$ and reference $|V_s^*|$ voltage magnitude, which is controlled by the voltage droop constant K_{vc}. The modulation signals i_{drmod} or i_{qrmod} are used to damp the inter-area oscillation as will be discussed in Section VI. For DC voltage control and reactive power control of the GSC (see Fig. 3), the stator terminal voltage vector is aligned with the q-axis. For a detailed state-space model of the DFIG, the readers are referred to [16].

In a NCPS remote feedback signals are used for power oscillation damping, which are sent through the communication network. Modeling of the communication channels and the uncertainties are discussed in the following section.

C. Modeling of Communication Network and Data Dropout

Reliable transmission of a continuous-time signal over a communication network constitutes the following steps: first, the signal must be sampled and encoded in a digital format, then transmitted over the network, and finally the data must

Copyright (c) 2017 IEEE. Personal use is permitted. For any other purposes, permission must be obtained from the IEEE by emailing pubs-permissions@ieee.org.

This is the author's version of an article that has been published in this journal. Changes were made to this version by the publisher prior to publication.
The final version of record is available at http://dx.doi.org/10.1109/TSG.2016.2631448

TABLE II
DIFFERENT DROPTOUT MODELS AND THEIR COMPLEXITY VS ACCURACY TRADEOFF

Model	*Parameter*	*Complexity*	*Simplification*
Bernoulli	p	*very low*	$k=1, h=0$
Simple Gilbert	p, r	*low*	$k=1, h \in \{0, 0.5\}$
Gilbert	p, r, h	*high*	$k=1$
Gilbert − Elliott	p, r, h, k	*very high*	–

be decoded at the receiver side. As shown in Fig. 1, in the communication network at the transmitting end, the transmitter consisting of an encoder maps the measurements into streams of bits that can be transmitted across the network and the receiver consist of a decoder at the receiving end, which maps the streams of bits received from the network into continuous signals. In our studies we did not explicitly represent the encoder and decoder - rather these are represented by zero-order-hold (ZOH) and sample and hold (S/H) circuits, respectively.

This work considers data dropout during communication, which is unpredictable. Characteristics of packet dropout over a network usually follows a stochastic process known as burst noise [17]. Fig. 4 shows different stochastic models of packet dropout whose complexity and accuracy are shown in Table II [18]. The most complex and detailed 2-state Markov process called the Gilbert-Elliott model is shown in Fig. 4(a). This model considers two states: the good (G) and the bad (B) states. Each of them may generate errors as independent events with the state dependent error rates, $1-k$ and $1-h$ in the good and the bad states, respectively. The transition probabilities between the states are defined by, p: G-state to B-state, r: B-state to G-state. The stationary state probabilities P_G and P_B exist for $0 < (p, r) < 1$ from which the error rate P_E and the packet delivery rate (R) of the transmission channel can be obtained in steady state as:

$$\begin{aligned} &P_G = r/(p+r), \quad P_B = p/(p+r) \\ &P_E = (1-k)P_G + (1-h)P_B \\ &R = (1-P_E) \times 100\% \end{aligned} \tag{3}$$

When $k=1$, the Gilbert-Elliott model is reduced to Gilbert model, Fig. 4(b). When $k=1$ and $h \in \{0, 0.5\}$ Gilbert model is reduced to simple Gilbert model, Fig. 4(c), and $k=1$, $h=0$ and $p+r=1$ gives the Bernoulli model, Fig. 4(d). This is the simplest dropout model.

As shown in Fig. 1, the estimated states $(\bar{x}(t))$ of the observer is sampled at times $\{t_k : k \in N\}$ and the samples $\bar{x}_k = \bar{x}(t_k)$ are sent through the communication network in the case of ORC approach discussed in Section IV. The corresponding data sample at the receiving end is denoted by $\bar{\bar{x}}(t)$. It is assumed that when the packet containing the sample $\bar{x}_k$ is dropped the NCS communication network utilizes the latest available sample $\bar{\bar{x}}_{k-1}$ in the receiving end. This corresponds to replacing the loss-less network model by: $\forall k \in N$

$$\bar{\bar{x}}_k = \mathbf{\Psi_k}\bar{x}_k + (I - \mathbf{\Psi_k})\bar{\bar{x}}_{k-1} \tag{4}$$

where $\mathbf{\Psi_k} = diag(\varphi_k^1, \varphi_k^2, ..., \varphi_k^n)$ is a binary diagonal random matrix and each φ_k^i follows a stochastic random variation with the understanding that $\varphi_k^i = 1$ (having a probability of $(1 - P_E)$) signifies that i^{th} element of the vector $\bar{x}_k$ reaches its destination and that $\varphi_k^i = 0$ (having a probability of P_E) when it does not. In this study $\varphi_k^i = \varphi_k^j$ for $i \neq j$ is assumed since all the elements of the vector $\bar{x}_k$ is part of same data packet.

III. CONVENTIONAL FEEDBACK CONTROL (CFC)

The test system, Fig. 2, has three poorly damped inter-area modes and the objective of the controllers is to damp these inter-area modes. As shown in Fig. 1 (in gray), a conventional feedback controller (CFC) measures signal $(y_m(t))$ from the remote PMUs that are communicated to the actuator location as $(\bar{y}_m(t))$. To establish this control function a Linear Quadratic Regulator (LQR) is located at the WF. To that end, a reduced order Luenberger type observer is used (see Fig. 1). The state-space model of the observer is given by:

$$\dot{\bar{x}}_{ob}(t) = A_n\bar{x}_{ob}(t) + B_n\bar{u}(t) + L(\bar{y}_m(t) - C_n\bar{x}_{ob}(t)) \tag{5}$$

where, L is the observer gain. The state-feedback control law is given by:

$$\bar{u}(t) = -K\bar{x}_{ob}(t) \tag{6}$$

Here $\bar{u}(t)$ is the modulating signal i_{drmod} or i_{qrmod} in Fig. 3 and K, the state-feedback controller gain vector calculated using LQR to minimize the control effort. Selection of control loop will be explained in Section VI-A.

Frequency of inter-area modes usually lie between $0.2-1.0$ Hz, therefore according to Nyquist-Shannon sampling theorem the minimum required sampling rate of the system is at least $2Hz$. In this paper, sampling rate of PMUs and the data transmission rate of the communication network are assumed to be $50Hz$ and $10Hz$, respectively. Damping electromechanical oscillations in NCPS using feedback signals from remote sensors is likely to be affected by occasional data dropout. Data dropout above a threshold could lead to unacceptable system response as illustrated in Section VI. When the data packets are dropped out in the communication link, special measures will be needed for oscillation damping control. Inspired by the model-based control philosophy in NCS literature [19], [20], an ORC approach is used in this work, which is described next.

IV. OBSERVER-DRIVEN REDUCED COPY (ORC) APPROACH

The Observer-driven Reduced Copy (ORC) approach exploits the knowledge of the nominal system to predict the dynamic behavior of the system when data packet drop occurs. The linearized power system model around the nominal operating point is reduced using the Schur balanced truncation approach [21] to the lowest possible order (10^{th} order) such that the reduced-order system (G_n) reasonably represents the dynamics of the full order system in the frequency range

Copyright (c) 2017 IEEE. Personal use is permitted. For any other purposes, permission must be obtained from the IEEE by emailing pubs-permissions@ieee.org.

This is the author's version of an article that has been published in this journal. Changes were made to this version by the publisher prior to publication.
The final version of record is available at http://dx.doi.org/10.1109/TSG.2016.2631448

of electromechanical modes. This reduced order model is described by:

$$G_n = \left[\begin{array}{c|c} A_n & B_n \\ \hline C_n & 0 \end{array}\right] \tag{7}$$

As shown in Fig. 1, an observer at the sensor location uses the reduced-order linearized model (G_n) of the system to estimate the states ($\bar{x}(t)$) described by:

$$\dot{\bar{x}}(t) = A_n\bar{x}(t) + B_n u(t) + L(y_m(t) - C_n\bar{x}(t)) \tag{8}$$

Estimates of the dynamic states $\bar{x}(t)$ is sent over the communication network instead of $y_m(t)$ to the WF. Control input signals ($u(t)$) at the actuator locations and the sensor locations are calculated using two reduced order models (G_n) of power system at each place (see Fig. 1). We call this model as the 'reduced copy of system model' or simply 'reduced copy'. The reduced copy dynamics and the control input signals ($u(t)$) are described by:

$$\begin{array}{l} \dot{x}_n(t) = A_n x_n(t) + B_n u(t) \\ u(t) = -K x_n(t) \end{array} \tag{9}$$

where K, the state-feedback controller gain vector, is calculated using LQR to minimize the control effort as discussed in Section III. When new data-packet is available, it is used to reset the dynamic states of the reduced copy in both sending and receiving ends at the same instant. Let the reduced copy at both locations be reset with the sample x^0_{nk} at time sample t_k satisfying:

$$x^0_{nk} = \mathbf{\Psi_k}\bar{x}_k + (I - \mathbf{\Psi_k})x_{nk} \tag{10}$$

where, x_{nk} is the dynamic state estimated by reduced copy when new data packets do not arrive. Since data dropout in the communication channel is a stochastic phenomena, the interval between two consecutive resetting $t_{k+1} - t_k = \Upsilon$ $\forall k = 0, 1, ...$ will encounter stochastic variations, thereby, resetting the states at unequal interval. When data packets drop out in the communication network and fails to reach the WF, the states of both the reduced copy are allowed to evolve naturally, otherwise the proposed architecture reset the states of both reduced copy, leading to a switched control strategy. This strategy is refereed as an ORC approach in this paper.

V. Analytical Derivation of Performance Affected by Cyber-Physical Coupling

Let us consider the reduced-order state-space model of the power system under off-nominal operating condition (e.g. line outage) denoted by:

$$G_i = \left[\begin{array}{c|c} A_i & B_i \\ \hline C_i & 0 \end{array}\right] \tag{11}$$

where, $A_i = A_n + \tilde{A}$, $B_i = B_n + \tilde{B}$, $C_i = C_n + \tilde{C}$ and $\tilde{A}$, $\tilde{B}$, $\tilde{C}$, represent the deviation around the nominal operating condition. The states of G_i is denoted as $x_i(t)$. Combining equations (8), (9) and the reduced-order power system dynamics under off-nominal condition from (11), one can derive the overall system dynamics during the time interval $t \in [t_k, t_{k+1})$, $t_{k+1} - t_k = \Upsilon$ as:

$$\begin{bmatrix} \dot{x}_i \\ \dot{x}_n \\ \dot{\bar{x}} \end{bmatrix} = \begin{bmatrix} A_i & -B_iK & 0 \\ 0 & A_n - B_nK & 0 \\ LC_i & -B_nK & A_n - LC_n \end{bmatrix} \begin{bmatrix} x_i \\ x_n \\ \bar{x} \end{bmatrix} \tag{12}$$

Accuracy of estimated states by the reduced copy would be affected when the system is under off-nominal conditions and communication channels have higher data dropout. Therefore, it would be useful to estimate the state trajectories of the reduced copy during the inter-sample interval. This section presents a derivation for the bound on the inter-sample error norm between the actual and the estimated states relating data dropout in the communication channel and model mismatch. Since data dropout is a stochastic phenomena, we are interested in the expectation on the bound. The expectation on the bound of this error is an indicator of the performance of ORC impacted by the cyber-physical interaction, which is derived next.

From the dynamics of the combined nominal, off-nominal and observer systems (12) during the inter-sample period $[t_k, t_{k+1})$, it is observed that the responses of $x_i(t)$ and $x_n(t)$ are uncoupled with that of the observer states $\bar{x}(t)$. Hence, the left upper block can be considered separately for analysis during $t \in [t_k, t_{k+1})$. Thus, neglecting the observer dynamics without loss of generality, (12) can be rewritten as:

$$\left[\begin{array}{c} \dot{x}_i(t) \\ \dot{x}_n(t) \end{array}\right] = \left[\begin{array}{cc} A_i & -B_iK \\ 0 & A_n - B_nK \end{array}\right] \left[\begin{array}{c} x_i(t) \\ x_n(t) \end{array}\right] \tag{13}$$

Let the initial conditions at sampling instant t_k be:

$$\left[\begin{array}{cc} x_i(t_k) & x_n(t_k) \end{array}\right]^T = \left[\begin{array}{cc} x^0_{ik} & x^0_{nk} \end{array}\right]^T$$

There is a finite probability associated with the resetting of reduced copy states by the estimated observer states $\bar{x}(t_k)$ according to (10). Solution of (13) for $t \in [t_k, t_{k+1})$ is given by:

$$\left[\begin{array}{c} x_i(t) \\ x_n(t) \end{array}\right] = e^{\Omega(t-t_k)} \left[\begin{array}{c} x^0_{ik} \\ x^0_{nk} \end{array}\right] \tag{14}$$

$$\text{where, } \Omega = \left[\begin{array}{cc} A_i & -B_iK \\ 0 & A_n - B_nK \end{array}\right] \tag{15}$$

Equation (14) represents the temporal evolution of the system states of the reduced order model and those of the reduced copy. The state trajectory of reduced copy with initial states x^0_{nk} can be expressed for $t \in [t_k, t_{k+1})$ as:

$$x_n(t) = e^{(A_n - B_nK)(t-t_k)}(\mathbf{\Psi_k}\bar{x}_k + (I - \mathbf{\Psi_k})x_{nk}) \tag{16}$$

To find the expression for the state trajectory of the reduced order linearized power system, equation (14) can be transformed into the Laplace domain as follows:

$$\left[\begin{array}{c} X_i(s) \\ X_n(s) \end{array}\right] = \mathcal{L}\{e^{\Omega(t-t_k)} \left[\begin{array}{c} x^0_{ik} \\ x^0_{nk} \end{array}\right]\} = \Lambda \left[\begin{array}{c} x^0_{ik} \\ x^0_{nk} \end{array}\right] \tag{17}$$

$$\Lambda = \left[\begin{array}{cc} (sI - A_i)^{-1} & \Delta \\ 0 & (sI - (A_n - B_nK))^{-1} \end{array}\right] \tag{18}$$

$$\Delta = -(sI - A_i)^{-1} B_i K (sI - A_n + B_nK)^{-1} \tag{19}$$

Copyright (c) 2017 IEEE. Personal use is permitted. For any other purposes, permission must be obtained from the IEEE by emailing pubs-permissions@ieee.org.

This is the author's version of an article that has been published in this journal. Changes were made to this version by the publisher prior to publication.
The final version of record is available at http://dx.doi.org/10.1109/TSG.2016.2631448

From (17), (18) and (19), $X_i(s)$ can be written as:

$$X_i(s) = (sI - A_i)^{-1}x_{ik}^0 + \Delta\, x_{nk}^0 \tag{20}$$

$$\begin{aligned} &= (sI - A_i)^{-1}x_{ik}^0 \\ &-(sI - A_i)^{-1}B_iK(sI - A_n + B_nK)^{-1}x_{nk}^0 \end{aligned} \tag{21}$$

$$\begin{aligned} &= (sI - A_n + B_nK)^{-1}x_{nk}^0 + (sI - A_i)^{-1}(x_{ik}^0 - x_{nk}^0) \\ &+(sI - A_i)^{-1}x_{nk}^0 - (sI - A_n + B_nK)^{-1}x_{nk}^0 \\ &-(sI - A_i)^{-1}B_iK(sI - A_n + B_nK)^{-1}x_{nk}^0 \end{aligned} \tag{22}$$

$$\begin{aligned} &= (sI - A_n + B_nK)^{-1}x_{nk}^0 + (sI - A_i)^{-1}(x_{ik}^0 - x_{nk}^0) \\ &+(sI - A_i)^{-1}(sI - A_n + B_nK)(sI - A_n + B_nK)^{-1}x_{nk}^0 \\ &-(sI - A_i)^{-1}(sI - A_i)(sI - A_n + B_nK)^{-1}x_{nk}^0 \\ &-(sI - A_i)^{-1}B_iK(sI - A_n + B_nK)^{-1}x_{nk}^0 \end{aligned} \tag{23}$$

$$\begin{aligned} &= (sI - A_n + B_nK)^{-1}x_{nk}^0 + (sI - A_i)^{-1}(x_{ik}^0 - x_{nk}^0) \\ &+(sI - A_i)^{-1}((sI - A_n + B_nK) - B_iK - (sI - A_i)) \\ &\times(sI - A_n + B_nK)^{-1}x_{nk}^0 \end{aligned} \tag{24}$$

After simplification (24) can be rewritten as:

$$\begin{aligned} X_i(s) &= (sI - A_n + B_nK)^{-1}x_{nk}^0 + (sI - A_i)^{-1}(x_{ik}^0 - x_{nk}^0) \\ &+(sI - A_i)^{-1}(\tilde{A} - \tilde{B}K)(sI - A_n + B_nK)^{-1}x_{nk}^0 \end{aligned} \tag{25}$$

From (10) and (25) the actual system states are given by:

$$\begin{aligned} x_i(t) &= e^{(A_n - B_nK)(t-t_k)}(\mathbf{\Psi_k}\bar{x}_k + (I - \mathbf{\Psi_k})x_{nk}) \\ &+e^{A_i(t-t_k)}(x_{ik}^0 - (\mathbf{\Psi_k}\bar{x}_k + (I - \mathbf{\Psi_k})x_{nk})) \\ &+\int_{t_k}^{t} e^{A_i(t-\tau)}(\tilde{A} - \tilde{B}K)e^{(A_n - B_nK)\tau} \\ &\times(\mathbf{\Psi_k}\bar{x}_k + (I - \mathbf{\Psi_k})x_{nk})d\tau \end{aligned} \tag{26}$$

The error between the reduced order linearized system state trajectory and that of reduced copy can be expressed as:

$$\begin{aligned} \xi(t) &:= x_i(t) - x_n(t) \\ &= e^{A_i(t-t_k)}(x_{ik}^0 - (\mathbf{\Psi_k}\bar{x}_k + (I - \mathbf{\Psi_k})x_{nk})) \\ &+\int_{t_k}^{t} e^{A_i(t-\tau)}(\tilde{A} - \tilde{B}K)e^{(A_n - B_nK)\tau} \\ &\times(\mathbf{\Psi_k}\bar{x}_k + (I - \mathbf{\Psi_k})x_{nk})d\tau \end{aligned} \tag{27}$$

One can re-write equation (27) as:

$$\begin{aligned} \xi(t) &= e^{A_i(t-t_k)}(x_{ik}^0 - \bar{x}_k) + e^{A_i(t-t_k)}(I - \mathbf{\Psi_k}) \\ &\times(\bar{x}_k - x_{nk}) + \int_{t_k}^{t} e^{A_i(t-\tau)}(\tilde{A} - \tilde{B}K)e^{(A_n - B_nK)\tau} \\ &\times(\mathbf{\Psi_k}(\bar{x}_k - x_{nk}) + x_{nk})d\tau \end{aligned} \tag{28}$$

The 2-norm inequality of the error $\xi(t)$ can be written as:

$$\begin{aligned} \|\xi(t)\| &\leq \left\|e^{A_i(t-t_k)}\right\| \left\|(x_{ik}^0 - \bar{x}_k)\right\| \\ &+ \left\|e^{A_i(t-\tau)}(\bar{x}_k - x_{nk})(I - \mathbf{\Psi_k})\right\| \\ &+ \left\|\int_{t_k}^{t} e^{A_i(t-\tau)}(\tilde{A} - \tilde{B}K)e^{(A_n - B_nK)\tau}\mathbf{\Psi_k}(\bar{x}_k - x_{nk})d\tau\right\| \\ &+ \left\|\int_{t_k}^{t} e^{A_i(t-\tau)}(\tilde{A} - \tilde{B}K)e^{(A_n - B_nK)\tau}\ x_{nk}d\tau\right\| \end{aligned} \tag{29}$$

Assuming a stable open-loop system, there are constants $k_1 > 0$ and $\delta_1 > 0$ such that for any vector $\gamma_1 \in \Re$:

$$\left\|e^{A_i t}\gamma_1\right\| \leq k_1 e^{-\delta_1 t}\left\|\gamma_1\right\| \tag{30}$$

Moreover, the closed-loop nominal system is stable and well-damped with the designed controller implying there exists constants $k_2 > 0$ and $\delta_2 > 0$ such that for any vector $\gamma_2 \in \Re$:

$$\left\|e^{(A_n - B_nK)t}\gamma_2\right\| \leq k_2 e^{-\delta_2 t}\left\|\gamma_2\right\| \tag{31}$$

Using (30) and (31) an estimate of the norm of the error $\xi(t)$ can be written as:

$$\begin{aligned} \|\xi(t)\| &\leq k_1\left\|(x_{ik}^0 - \bar{x}_k)\right\| e^{-\delta_1(t-t_k)} \\ &+k_1\left\|I - \mathbf{\Psi_k}\right\|\left\|\bar{x}_k - x_{nk}\right\| e^{-\delta_1(t-t_k)} \\ &+k_1k_2\left\|(\tilde{A} - \tilde{B}K)\right\|(\left\|\mathbf{\Psi_k}\right\|\left\|\bar{x}_k - x_{nk}\right\| + \left\|x_{nk}\right\|) \\ &\times\int_{t_k}^{t} e^{-\delta_1(t-\tau)}e^{-\delta_2\tau}d\tau \end{aligned} \tag{32}$$

Equation (32) further simplifies to:

$$\begin{aligned} \|\xi(t)\| &\leq k_1\left\|(x_{ik}^0 - \bar{x}_k)\right\| e^{-\delta_1(t-t_k)} \\ &+k_1\left\|I - \mathbf{\Psi_k}\right\|\left\|\bar{x}_k - x_{nk}\right\| e^{-\delta_1(t-t_k)} \\ &+k_1k_2\left\|(\tilde{A} - \tilde{B}K)\right\|(\left\|\mathbf{\Psi_k}\right\|\left\|\bar{x}_k - x_{nk}\right\| + \left\|x_{nk}\right\|) \\ &\times\frac{[e^{-\delta_2(t-t_k)} - e^{-\delta_1(t-t_k)}]}{(\delta_1 - \delta_2)e^{\delta_2 t_k}} \end{aligned} \tag{33}$$

Note: In equations (24), (26), (27), (28), (32), and (33) the symbol '$\times$' is used to denote matrix multiplications since two multiplicative terms could not be accommodated in the same line. This is otherwise omitted from equations.

Assuming $(x_{ik}^0 - \bar{x}_k) = 0$, i.e. that the observer tracks the actual states perfectly, one can derive an approximated expression for the bound on the inter-sample error norm as:

$$\begin{aligned} \|\xi(t)\|_{max} \propto K_1\left\|I - \mathbf{\Psi_k}\right\| + K_2\left\|\tilde{A} - \tilde{B}K\right\| \\ +K_3\left\|\tilde{A} - \tilde{B}K\right\|\left\|\mathbf{\Psi_k}\right\| \end{aligned} \tag{34}$$

where constant K_1, K_2 and $K_3 \in \Re$. There is a probability associated with $\xi(t)$ in the interval $t \in [t_k, t_{k+1})$ since it is *not deterministic* that the new data sample will be available and the reduced copy will be reset at t_k. The probability associated with resetting at t_k is:

$$\mathbf{P}(\mathbf{\Psi_k} = I) = \boldsymbol{\rho} = R/100 = \text{data receiving rate.} \tag{35}$$

Using (35) the expected value of $\|\xi(t)\|_{max}$ can be derived as:

$$\begin{aligned} \mathbf{E}[\|\xi(t)\|_{max}] \propto K_1(1 - \boldsymbol{\rho}) + K_2\left\|\tilde{A} - \tilde{B}K\right\| \\ +K_3\left\|\tilde{A} - \tilde{B}K\right\|\boldsymbol{\rho} \end{aligned} \tag{36}$$

□ **Discussion on cyber-physical coupling**: It can be seen from (36) that the expectation of the maximum norm of error is proportional to the data drop out in the communication link (1^{st} term), the norm of model mismatch (2^{nd} term) and the model mismatch norm coupled with the data receiving rate (3^{rd} term). Noteworthy points are:

- impact of cyber-only term indicates the error norm increases with increase in data dropout, which is expected
- impact of physical-only term indicates increase in error norm under off-nominal condition, which is expected
- the cyber-physical coupling term indicates a non-trivial impact on the error norm

This reveals the impact of the interaction between the cyber and the physical layer on the ORC performance, which will be verified by time-domain simulation in section VI-B.3.

Copyright (c) 2017 IEEE. Personal use is permitted. For any other purposes, permission must be obtained from the IEEE by emailing pubs-permissions@ieee.org.

This is the author's version of an article that has been published in this journal. Changes were made to this version by the publisher prior to publication.
The final version of record is available at http://dx.doi.org/10.1109/TSG.2016.2631448

TABLE III
COMPARISON OF INTER-AREA MODES OF THE SYSTEMS WITH SG-PSS, DFIG AND DFIG-PSS

Scenarios	$SG-PSS$		$DFIG-G9$		$DFIG$ $G9$ & $G15$		$DFIG-PSS$ ($G9$ & $G15$)	
Modes	T_s, s	f, Hz	T_s, s	f, Hz	T_s, s	f, Hz	T_s, s	f, Hz
#1	25.7	0.38	113.6	0.40	69.4	0.42	10.6	0.42
#2	28.9	0.50	29.5	0.50	28.3	0.51	12.2	0.51
#3	18.0	0.62	22.7	0.62	22.5	0.62	10.4	0.62
#4	16.1	0.79	16.1	0.79	–	–	–	–

Relative mode shapes of generator speeds for four inter-area modes when G9 and G15 are SGs

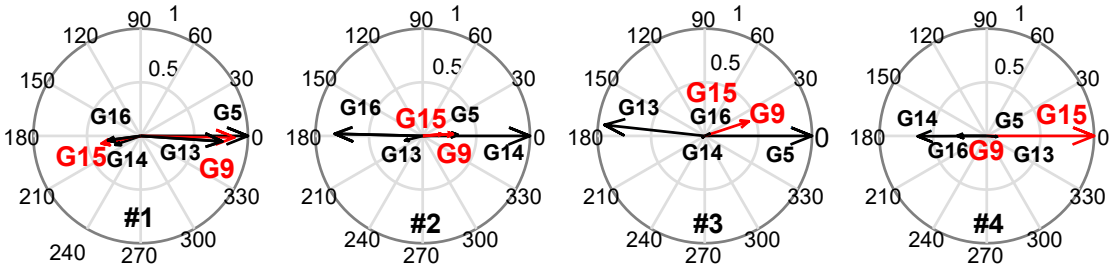

Relative mode shapes of generator speeds for four inter-area modes when G9 is DFIG and G15 is SG

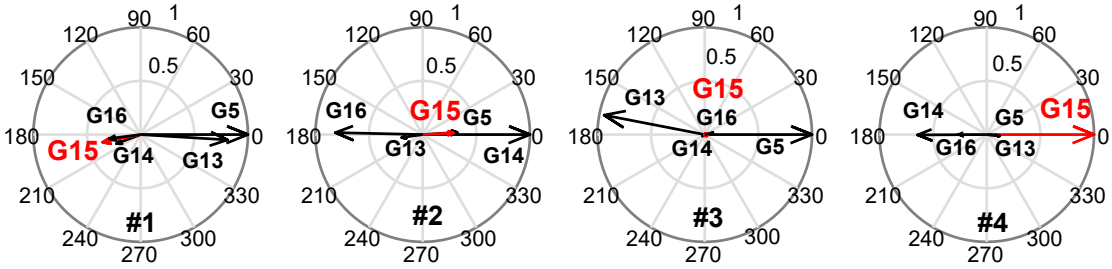

Relative mode shapes of generator speeds for three inter-area modes when G9 and G15 are DFIGs

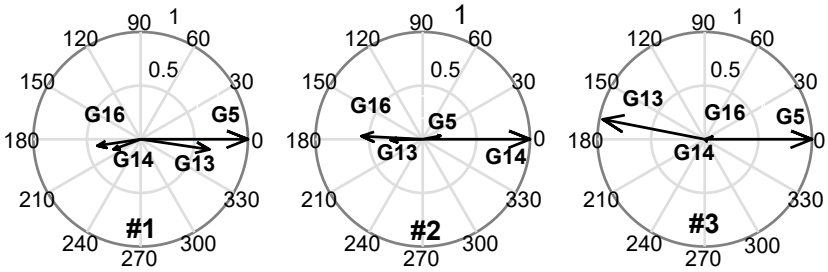

Fig. 5. Relative mode shapes of generator speeds for four inter-area modes where G9 and G15 (red arrows) are either SGs or DFIGs. Generators from each area with the highest participation are shown. #1, #2, #3, and #4 denote the modes #1, #2, #3, and #4, respectively. When G15 is replaced by a DFIG, the mode #4 ceased to exit.

□ **Comment**: It is worth noting that, when the open loop system is unstable the second term in equation (29) will exponentially increase with time in presence of data drop, i.e. the inter-sample error norm will become unbounded. This could be possible under operating conditions when cascaded contingencies involving (N-2) or (N-3) outages take place. Fortunately, system planners in power system ensures that the grid is stable under a wide range of operating conditions and following all (N-1) outage scenarios. This determines the operating envelop, which considers load growth in 5 to 10 years of planning horizon. This is mandated by The North American Electric Reliability Corporation (NERC). Therefore, it is highly unlikely that the system (i.e. the open loop system) will become unstable following an (N-1) contingency under loading conditions within the operating envelop.

VI. SIMULATION RESULTS AND DISCUSSION

To validate the effectiveness of the proposed ORC approach under different data dropout scenarios in a smart power grid the 16-machine test system shown in Fig. 2 is considered. The following sections present analysis and simulation results in Matlab/Simulink platform.

Copyright (c) 2017 IEEE. Personal use is permitted. For any other purposes, permission must be obtained from the IEEE by emailing pubs-permissions@ieee.org.

This is the author's version of an article that has been published in this journal. Changes were made to this version by the publisher prior to publication.
The final version of record is available at http://dx.doi.org/10.1109/TSG.2016.2631448

A. Modal Analysis and Control Loop Selection

As shown in Table III, the linearized system with SG and PSS at bus 9, Fig. 2, denoted by SG-PSS has four inter-area modes with frequencies in the range of $0.3 - 0.8\ Hz$. When the SG with PSS at G9 is replaced by DFIG, the settling time (T_s) of three inter-area modes (mode #1, #2 and #3) become poorer while mode #4 remains unaffected. When G15 is also replaced by DFIG, settling time of the inter-area modes remain unacceptably high and mode #4 ceased to exit, see Table III. To explain the absence of mode #4 the mode shapes of the generator speeds for all four modes are shown in Fig. 5. Generators from each area with the highest participation are shown here. It can be seen from Fig. 5 that in mode #4, SG G15 oscillates against the rest of the generators in the system. When the SG is replaced by a DFIG-based wind farm, the faster controls in the RSC tightly regulates the generator speed for MPPT, which prevents the DFIG in participating in the inter-area modes. Since in this condition G15 does not oscillate against the rest of the generators in the system, this particular inter-area mode ceases to exist. This reaffirms the findings of reference [22].

Unacceptably high settling times of the inter-area modes indicate need of PSSs at G9 and G15. As discussed in Section II-B, current control strategy is used for the RSC of DFIG, Fig.3. Therefore, the d and q components of the rotor currents are selected as the modulation signals. Based upon the modal controlability of rotor currents i_{drmod} of G9 and i_{qrmod} of G15 are selected as the control input.

The control objective of the DFIG-PSS is to improve the damping of the inter-area oscillations of the system using modulation signals of rotor current. A SISO controller is used at each actuator location (G9 and G15) to meet these control objectives. The modal observability of local and remote feedback signals reveal that the DFIG stator power P_{G9} and P_{G15} are not suitable for effective damping performance. In this case power flows P_{27-37} and P_{14-41} are selected as the feedback signals ($y_m(t)$) based on residue magnitude-angle criteria mentioned in [23] for $G9$ and $G15$, respectively. The observability magnitudes (normalized) of P_{14-41} are: 0.2 (mode #1), 1.0 (mode #2), and 0.02 (mode #3) and the corresponding values for P_{27-37} are: 0.1, 0.02, and 0.08, respectively. The controllers are designed using LQR approach as explained in Section III. The SISO controller for each WF was designed using a sequential approach mentioned in [13]. As shown in Table III, DFIG-PSS achieves settling times of less than 15.0 s for all three modes. Next, the impact of data-packet drop in the communication network and the off-nominal operating conditions on the effectiveness of the proposed ORC approach (Section IV) over the CFC (Section III) is analyzed.

B. Performance of ORC Compared to CFC

Feedback signals P_{27-37} and P_{14-41} are communicated to the sites of the WFs and independent stochastic data packet-drop models are used for each communication channel. As proposed in Section IV, the ORC is embedded in each control loop. Nonlinear time-domain simulations are performed under different operating conditions and data receiving rates (R) in the communication channel, see equation (3). The values of $p = 0.0277$, and $r = 0.25$ are used for all cases. The values of $h = 0.51, 0.5$, and 0.43 along with $k = 0.775, 0.5$, and 0.25 are chosen for $R = 25, 50$, and 75%, respectively. The values of p and r are chosen from the paper [17], as mentioned in [17] the value of h is selected around 0.5, and k can be calculated using equation (3) to attain the desired data receiving rates of 75, 50, and 25% in the communication channel. For more information regarding selection of the parameters the readers are referred to [17], [18].

1). **Effect of Communication Data Dropouts on ORC:** A three-phase self-clearing fault near bus 60, Fig. 2, is considered to evaluate damping performance in the nominal condition. The system response with ORC for data receiving rates of $100, 50$, and 25% is compared against CFC response with 50 and 25% receiving rates, see Fig. 6. The following observations can be made:

- CFC becomes unstable below a certain data receiving rate for which ORC produces satisfactory damping performance.
- The performance of ORC is almost similar for $25, 50$, and 100% data receiving rates following self-clearing faults.

2). **Impact of Operating Condition Coupled with Comm--unication Data Dropouts on ORC:** Since the control design and the reduced copy is based on the nominal condition, it would affect the behavior of ORC under off-nominal operating condition (e.g. following line outages). To study the effect of the operating condition on the ORC performance, system response after a three-phase fault near bus 18 followed by the outage of one of the tie-lines between buses 18 and 42 is considered, Figs 7 and 8. Two more case studies involving fault near bus 60 followed by line $60 - 61$ outage and fault near bus 40 followed by line $40 - 41$ outage are also shown in Figs 7 and 8. For each case, the performance of ORC is compared against that of CFC for different data receiving rates. It can be observed that:

- When $R = 100\%$, the closed-loop performance with ORC becomes marginally poorer compared to the nominal condition.
- Satisfactory damping performance under different operating conditions indicates a reasonable robustness of the controller.

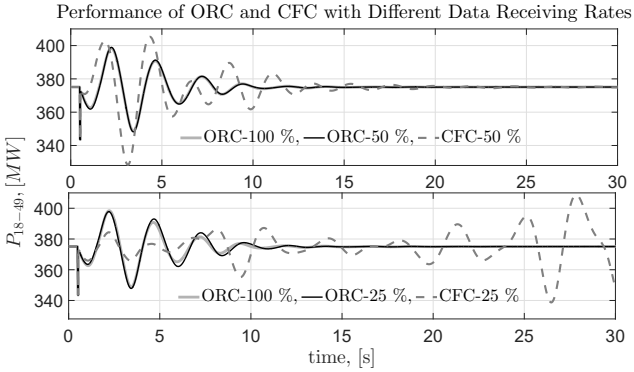

Fig. 6. Comparison of the CFC versus ORC with different data receiving rates (R) for a self-clearing fault near bus 60, see Fig. 2.

Copyright (c) 2017 IEEE. Personal use is permitted. For any other purposes, permission must be obtained from the IEEE by emailing pubs-permissions@ieee.org.

This is the author's version of an article that has been published in this journal. Changes were made to this version by the publisher prior to publication.
The final version of record is available at http://dx.doi.org/10.1109/TSG.2016.2631448

TABLE IV
THE VALUES OF NORM TERMS IN THE EQUATION (36) FOR DIFFERENT OUTAGES AND DATA PACKET DROPOUT. NOTE: K_1, K_2, AND K_3 CANNOT BE QUANTIFIED

Outage		*Case I* : $R = 25\%$		*Case II* : $R = 50\%$		*Case III* : $R = 75\%$	
	$\|\tilde{A} - \tilde{B}K\|$	$(1-\boldsymbol{\rho})$	$\boldsymbol{\rho}\|\tilde{A} - \tilde{B}K\|$	$(1-\boldsymbol{\rho})$	$\boldsymbol{\rho}\|\tilde{A} - \tilde{B}K\|$	$(1-\boldsymbol{\rho})$	$\boldsymbol{\rho}\|\tilde{A} - \tilde{B}K\|$
$18-42$	6.0863×10^4	0.7486	1.5303×10^4	0.5000	3.0431×10^4	0.2680	4.4554×10^4
$60-61$	4.9036×10^4	0.7486	1.2329×10^4	0.5000	2.4518×10^4	0.2680	3.5897×10^4
$40-41$	4.5554×10^4	0.7486	1.1454×10^4	0.5000	2.2777×10^4	0.2680	3.3348×10^4

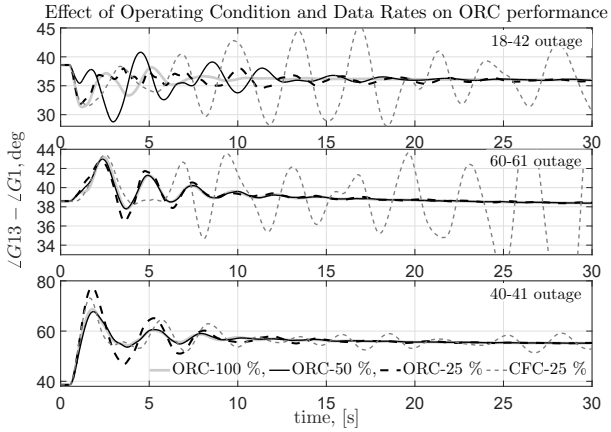

Fig. 7. Dynamic performance after a three-phase fault near bus $18/60/40$ following by the outage of one of the tie-lines between buses $18-42/60-61/40-41$, respectively, see Fig. 2.

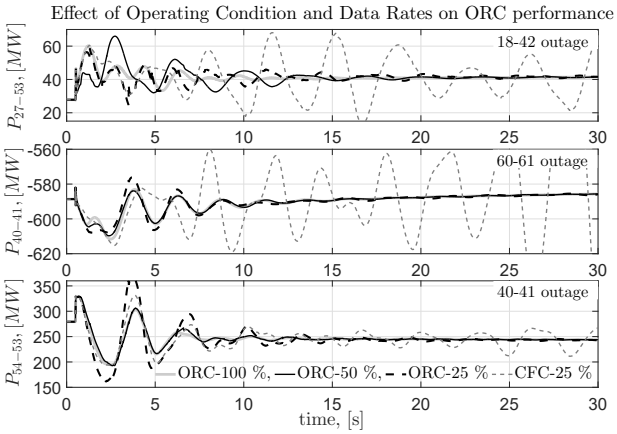

Fig. 8. Dynamic performance after a three-phase fault near bus $18/60/40$ following by the outage of one of the tie-lines between buses $18-42/60-61/40-41$, respectively, see Fig. 2.

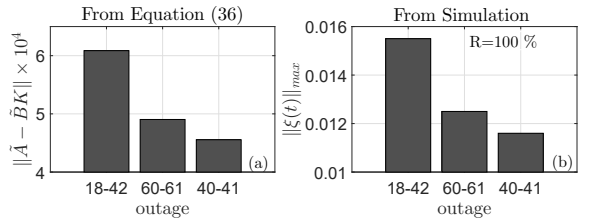

Fig. 9. Bound on error norm of state trajectories in the inter-sample interval with ideal communication channel: (a) measure of bound on error norm from equation (36), (b) calculated bound on error from linear simulation.

- With high data dropout rates ORC performance is slightly poorer than that of the ideal communication scenario. On the other hand the CFC results in unacceptable response with high data dropout rate.

3). **Time-Domain Simulation for Error Norm Validation:**
It is not straightforward to quantitatively correlate the trends in simulation with the analysis in Section V primarily due to the effect of nonlinearities and model reduction. To avoid this issue, time-domain simulation was conducted using the reduced order linear model of the system. Under ideal communication scenario (i.e. $R = 100\%$), the measure of bound on error norm from equation (36) is shown in Fig. 9.(a). The error bound of state trajectories in the inter-sample interval calculated from the linear time-domain simulation for different outage scenarios are shown in Fig. 9.(b), which correlates with measures in Fig. 9.(a) in a relative sense.
To characterize the dispersion of the bound on the inter-sample error norm under different data dropout and line-outage scenarios, 100 Monte Carlo runs were conducted for each line outage under each value of $R = 75, 50$, and 25%, respectively. Therefore, total 900 such simulations were run. For a particular value of data receiving rate R, the diagonal matrix $\boldsymbol{\Psi}_{\mathbf{k}}$ (all zero or all one), associated with probability P_E is sampled by randomizing the sequence. The simulation results are summarized in the form of boxplots in Fig. 10 whose mean values are indicative of $\mathbf{E}[\|\xi(t)\|_{max}]$ in equation (36) and the values of norm terms in the equation (36) for different outages and data packet dropout are shown in Table IV. Please note that K_1, K_2, and K_3 cannot be quantified. It can be concluded from Fig. 10 that:

- $\mathbf{E}[\|\xi(t)\|_{max}]$ increases for each outage with reduction in data rate R.
- The effect of data rate R and change in operating condition denoted by $\left\|\tilde{A} - \tilde{B}K\right\|$ are coupled with conflicts between the first and the third terms, see equation (36). As a results, the trend of $\mathbf{E}[\|\xi(t)\|_{max}]$ across different outages do not follow the trend in ideal communication scenarios shown in Fig. 9.

The objective of this exercise was to validate whether the proposed ORC approach behaves as expected from the linear control theory.

4). **Impact of latency and measurement noise:**
Figure 11.(a) shows the performance of ORC under $150-ms$ delay in the communication channel. In the second case study band-limited Gaussian measurement noise is added to each feedback signal shown in Fig. 11.(b). The performance of ORC in presence of measurement noise is shown in Fig. 11.(c).

Copyright (c) 2017 IEEE. Personal use is permitted. For any other purposes, permission must be obtained from the IEEE by emailing pubs-permissions@ieee.org.

This is the author's version of an article that has been published in this journal. Changes were made to this version by the publisher prior to publication.
The final version of record is available at http://dx.doi.org/10.1109/TSG.2016.2631448

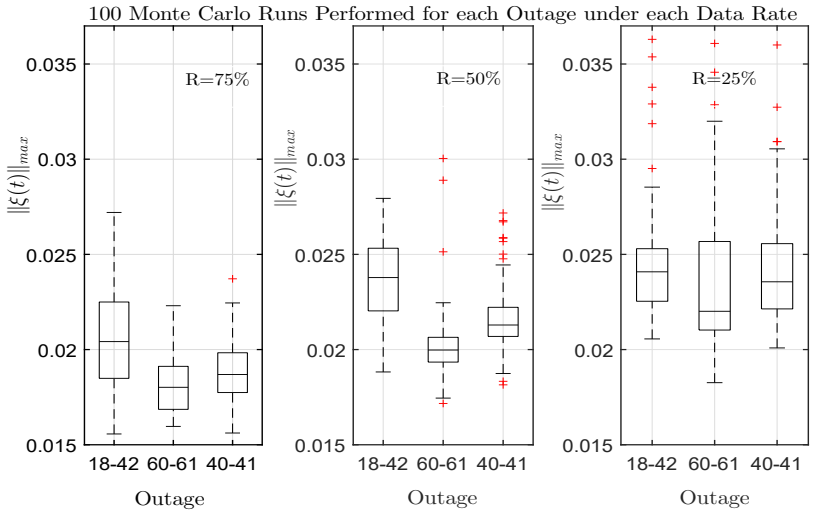

Fig. 10. Boxplots of maximum error bound of state trajectories in the inter-sample interval with non-ideal communication channel calculated from linear time-domain simulation. 100 Monte Carlo runs were conducted for each outage under data rate, i.e. total 900 runs were performed.

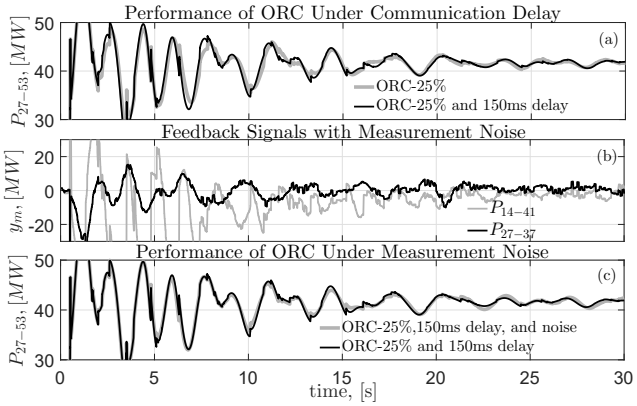

Fig. 11. Dynamic performance after a three-phase fault near bus 18 following by the outage of one of the tie-lines between buses $18-42$, see Fig. 2: (a) performance of ORC under delay in the communication channels, (b) the feedback signals with measurement noise. The washout block is used to remove the DC offset from the signals, (c) performance of ORC under delay and the measurement noise.

Satisfactory damping performance under communication delay and measurement noise is observed.

VII. Conclusion

The Gilbert-Elliot model was used for representing stochastic data packet drop in communication system for wide-area damping control using multiple DFIG-based wind farms. An Observer-driven Reduced Copy (ORC) approach is presented to deal with the packet dropouts in a networked control framework. An analytical expression is derived to quantify the impact of interaction between the uncertainty in cyber layer due to data drop and off-nominal operation of the grid, i.e., the physical layer due to outages. Monte Carlo simulation results from linear model validate the impact of data drop, the change in operating conditions, and their coupling. Nonlinear simulations demonstrate the effectiveness of ORC approach in handling packet drops, delay in the communication channel, and the measurement noise.

Appendix I: Control Parameters

A. For wind farm at G9

$$K = [0.1386, 0.0543, -0.2587, -0.2080, 0.6985, -1.0741, 0.0870, -0.5498, 0.2722, -0.1257]$$
$$L = 1 \times 10^5 \times [0.0233, -1.1779, -0.4473, 0.6017, 0.3204, 0.1646, -0.0950, -0.0673, -0.0120, 0.0142]^T \quad (37)$$

B. For wind farm at G15

$$K = [4.5723, 0.8211, 1.6110, 0.3284, 0.3678, 0.3211, -0.2893, 0.4152, -0.0888, 0.1160]$$
$$L = 1 \times 10^4 \times [0.2303, 0.9877, -1.1633, 0.1201, 0.1081, -0.4972, -0.3218, -0.0320, -0.0523, 0.0373]^T \quad (38)$$

References

[1] American Physical Society's Panel on Public Affairs (POPA), "Integrating Renewable Electricity on the Grid", Tech. Rep., Nov 2010.
[2] J. Hespanha, P. Naghshtabrizi, and Y. Xu, "A survey of recent results in networked control systems," *Proceedings of the IEEE*, vol. 95, pp. 138–162, 2007.
[3] L. A. Montestruque and P. Antsaklis, "Stability of model-based networked control systems with time-varying transmission times," *IEEE Transactions on Automatic Control*, vol. 49, no. 9, pp. 1562–1572, 2004.
[4] M. S. Branicky, "Stability of switched and hybrid systems," in *Proceedings of the 33rd IEEE Conference on Decision and Control*.
[5] G. C. Walsh, Y. Hong, and L. G. Bushnell, "Stability analysis of networked control systems," *IEEE Transactions on Control Systems Technology*, vol. 10, no. 3, pp. 438–446, 2002.
[6] W. Wing Shing and R. W. Brockett, "Systems with finite communication bandwidth constraints. I. state estimation problems," *IEEE Transactions on Automatic Control*, vol. 42, no. 9, pp. 1294–1299, 1997.
[7] ——, "Systems with finite communication bandwidth constraints. II. stabilization with limited information feedback," *IEEE Transactions on Automatic Control*, vol. 44, no. 5, pp. 1049–1053, 1999.
[8] M. Mokhtari and F. Aminifar, "Toward wide-area oscillation control through doubly-fed induction generator wind farms," *IEEE Transactions on Power Systems*, vol. 29, pp. 2985–2992, 2014.
[9] A. E. Leon and J. A. Solsona, "Power oscillation damping improvement by adding multiple wind farms to wide-area coordinating controls," *IEEE Transactions on Power Systems*, vol. 29, pp. 1356–1364, 2014.

Copyright (c) 2017 IEEE. Personal use is permitted. For any other purposes, permission must be obtained from the IEEE by emailing pubs-permissions@ieee.org.

This is the author's version of an article that has been published in this journal. Changes were made to this version by the publisher prior to publication.
The final version of record is available at http://dx.doi.org/10.1109/TSG.2016.2631448

[10] T. Surinkaew and I. Ngamroo, "Hierarchical co-ordinated wide area and local controls of dfig wind turbine and pss for robust power oscillation damping," *IEEE Transactions on Sustainable Energy*, vol. 7, pp. 943–955, 2016.
[11] N. R. Chaudhuri, D. Chakraborty, and B. Chaudhuri, "An architecture for FACTS controllers to deal with bandwidth-constrained communication," *IEEE Transactions on Power Delivery*, vol. 26, no. 1, pp. 188–196, 2011.
[12] A. Singh, R. Singh, and B. Pal, "Stability analysis of networked control in smart grids," *IEEE Transactions on Smart Grid*, vol. 6, pp. 381–390, 2015.
[13] B. Pal and B. Chaudhuri, *Robust control in power systems*, ser. Power electronics and power systems. New York: Springer, 2005.
[14] J. G. Slootweg, H. Polinder, and W. L. Kling, "Dynamic modelling of a wind turbine with doubly fed induction generator," in *Power Engineering Society Summer Meeting*, vol. 1, 2001.
[15] R. Pena, J. C. Clare, and G. M. Asher, "Doubly fed induction generator using back-to-back PWM converters and its application to variable-speed wind-energy generation," *IEE Proceedings on Electric Power Applications*, vol. 143, no. 3, pp. 231–241, 1996.
[16] A. Yogarathinam, J. Kaur, and N. R. Chaudhuri, "Impact of inertia and effective short circuit ratio on control of frequency in weak grids interfacing LCC-HVDC and DFIG-based wind farms," *IEEE Transactions on Power Delivery*, pp. 1–11, 2016.
[17] E. K. Gilbert, "Capacity of a burst-noise channel," *Bell Sys. Tech. Journal*, vol. 39, p. 1253, Sept 1960.
[18] G. Hasslinger and O. Hohlfeld, "The gilbert-elliott model for packet loss in real time services on the internet," in *14th GI/ITG Conference - Measuring, Modelling and Evaluation of Computer and Communication Systems (MMB)*, 2008.
[19] L. A. Montestruque and P. J. Antsaklis, "On the model-based control of networked systems," *Automatica*, vol. 39, no. 10, pp. 1837–1843, 2003.
[20] P. V. Zhivoglyadov and R. H. Middleton, "Networked control design for linear systems," *Automatica*, vol. 39, no. 4, pp. 743–750, 2003.
[21] S. Skogestad and I. Postlethwaite, *Multivariable feedback control: analysis and design*. Chichester: Wiley, 1996.
[22] J. J. Sanchez-Gasca, N. W. Miller, and W. W. Price, "A modal analysis of a two-area system with significant wind power penetration," in *IEEE PES Power Systems Conference and Exposition.*, vol. 2, 2004.
[23] S. Ray, B. Chaudhuri, and R. Majumder, "Appropriate signal selection for damping multi-modal oscillations using low order controllers," in *IEEE Power and Energy Society General Meeting - Conversion and Delivery of Electrical Energy in the 21st Century*, 2008.

Amirthagunaraj Yogarathinam (S'12) received his B.E. degree in Electrical and Electronic Engineering from University of Peradeniya, Sri Lanka in 2013. He is currently pursuing the Ph.D. degree at The Pennsylvania State University, PA, USA. He was a Researcher and Instructor in the Department of Electrical and Electronic Engineering, University of Peradeniya, Peradeniya, Sri Lanka, from 2013 to 2014. His research interests include power system dynamics and control, HVDC, wind power integration to the modern grid, wide-area monitoring and control, application of power electronics in power systems, online system identification, nonlinear system and control, and smart grid.

Nilanjan Ray Chaudhuri (S'08-M'09-SM'16) received his Ph.D. degree from Imperial College London, London, UK in 2011 in Power Systems. From 2005-2007, he worked in General Electric (GE) John F. Welch Technology Center. He came back to GE and worked in GE Global Research Center, NY, USA as a Lead Engineer during 2011-2014. Presently, he is an Assistant Professor with the School of Electrical Engineering and Computer Science at Penn State, University Park, PA. He was an Assistant Professor with North Dakota State University, Fargo, ND, USA during 2014-2016. He is a member of the *IEEE* and *IEEE PES*. Dr. Ray Chaudhuri is the lead author of the book *Multi-terminal Direct Current Grids: Modeling, Analysis, and Control* (Wiley/IEEE Press, 2014), and an Associate Editor of the IEEE TRANSACTIONS ON POWER DELIVERY. Dr. Ray Chaudhuri is the recipient of the National Science Foundation Early Faculty CAREER Award in 2016.

Copyright (c) 2017 IEEE. Personal use is permitted. For any other purposes, permission must be obtained from the IEEE by emailing pubs-permissions@ieee.org.